

Spherical deformation of compliant substrates with semiconductor device islands

P. I. Hsu,^{a)} M. Huang, Z. Xi,^{b)} S. Wagner, Z. Suo,^{c)} and J. C. Sturm
*Center for Photonics and Optoelectronic Materials (POEM), Princeton University,
 Princeton, New Jersey 08544*

(Received 13 June 2003; accepted 27 October 2003)

This article explores, through experiments and finite element analysis, the ability to plastically deform thin-film semiconductor structures on deformable substrates to spherical cap shapes without cracking the semiconductor layers. The major challenge involves contending with the large strain due to extreme deformation that will crack uniform stiff layers, such as silicon or silicon nitride. By patterning amorphous silicon and silicon nitride layers into islands, such problems can be avoided despite average strains in the substrate in excess of 5%. The strain in the device islands after deformation is a function of the island structure, size, and substrate material properties. Although the substrate is plastically expanded to a spherical dome, device islands can experience either tension or compression depending on the structure. © 2004 American Institute of Physics.

[DOI: 10.1063/1.1634370]

I. INTRODUCTION

The applications of traditional large-area electronics, such as displays, are limited by the fact that glass substrates are rigid and easily breakable. Large-area electronics, such as electronic paper, sensor skin, and electrotexiles, requires building electronic devices on flexible and deformable substrates.^{1–5} Substrates, such as organic polymers and stainless-steel foils, can be deformed into arbitrary shapes, but inorganic semiconductor device materials, such as amorphous silicon and silicon nitride, are brittle and crack easily when substrates are deformed. Therefore, to achieve flexible electronics, it is essential to reduce the applied mechanical strain in such device structure on deformable substrates. Most of the work to date has focused on cylindrical deformation of thin foil substrates. In such cases, the semiconductor films on the inside of the deformed surface are in compression and those on the outside are in tension, while there exists a plane between these two with no strain (neutral plane).^{4,5} Assuming the film thickness is negligible and the neutral plane is at the midsurface of the substrate, the magnitude of strain in the surfaces is given by

$$\varepsilon_{\text{uniaxial}} = \frac{t}{2\rho}, \quad (1)$$

where t is the substrate thickness and ρ is the radius of curvature. Since the surface strain can be decreased by reducing the substrate thickness, tight radii of curvature can be achieved simply by using thinner substrates.

In this article, we report work aiming toward the permanent deformation of thin-film electronics, first fabricated by

conventional methods on flat foil substrates, into a spherically shaped cap after the device fabrication process. In contrast to rolling, with spherical deformation, the surface is in tension on both the concave and convex sides of the substrate and thinning the substrate cannot be used to reduce the strain. Because inorganic semiconductor materials are brittle, the uniform layers of device materials crack during the substrate deformation. Thus, spherical deformation is fundamentally more difficult than cylindrical deformation because the deformation inherently involves stretching the substrate and devices on it, independent of the substrate thickness.

In this article, Sec. II explains our approach to plastically deform thin foil substrates into spherical dome shapes. Section III demonstrates that by patterning device materials into isolated islands, “hard” device islands can remain crack free after deformation. Finally, Sec. IV discusses that the strain distribution in the device islands for two different substrate structures, and why patterning brittle materials into islands suppresses fracture in the devices.

II. SUBSTRATE DEFORMATION

In our experiments, pressurized gas is used to deform structures on thin foil stainless-steel or Kapton™ polyimide substrates, which are clamped at the edges (6 cm in diameter), into spherically shaped caps.⁶ By comparing the initial foil cross section with the final deformed arc (Fig. 1), the average radial strain ($\varepsilon_{r,\text{avg}}$) necessary to expand the foil to a spherical shape subtending a given angle (θ) is

$$\varepsilon_{r,\text{avg}} = \frac{\frac{\theta}{2} - \sin \frac{\theta}{2}}{\sin \frac{\theta}{2}} = \frac{\sin^{-1} \left(\frac{2Rh}{R^2 + h^2} \right) - \frac{2Rh}{R^2 + h^2}}{\frac{2Rh}{R^2 + h^2}} \approx \frac{\theta^2}{24} = \frac{2}{3} \left(\frac{Rh}{R^2 + h^2} \right)^2. \quad (2)$$

In practice, we measured the height of deformation at the center of the foil (h) and the radius (R) of the clamped region

^{a)} Author to whom correspondence should be addressed; electronic mail: irishsu@iee.org

^{b)} Present address: Center for Composite Materials, University of Delaware, Newark, DE 19716.

^{c)} Present address: Division of Engineering and Applied Sciences, Harvard University, Cambridge, MA 02138.

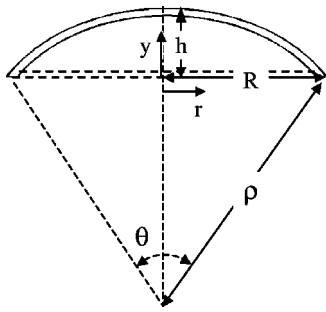


FIG. 1. Schematic cross section of the foil before and after deformation, where θ is the field of view, h is the height of the spherical dome, R is the radius of the clamped substrate, and ρ is the radius of curvature.

to estimate the average radial strain in the substrate. For a 66° field-of-view spherical dome, which subtends a solid angle of one steradian, the average radial strain is 5.6%. This also corresponds $h/R=0.29$. We use this model benchmark as a goal for most of the work in this article.

A. Steel substrates

We first experimented with bare stainless-steel foils (AISI 316, 12.5 μm or 25 μm thick), which were plastically deformed by nitrogen pressurized up to 345 kPa (50 psi). At 345 kPa, the center of 12.5- μm -thick foil was raised by ~ 0.50 cm ($h/R=0.17$) [Fig. 2(b), Sample B], corresponding

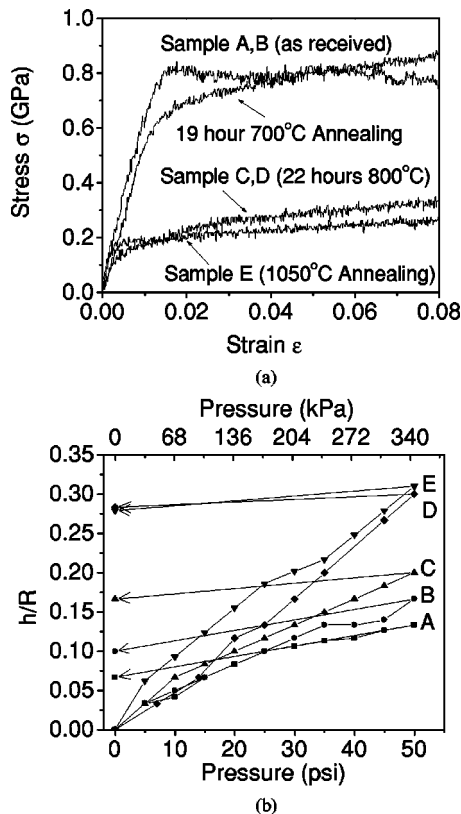


FIG. 2. (a) Measured stress–strain relationship for the stainless-steel sheets. Annealing reduced the yield strength of the steel foils. (b) Height of deformed stainless-steel sheets as a function of applied pressure, with the height at the center of spherical domes normalized by the radius of the deformed region R (as defined in Fig. 1). The pressure was increased from zero.

TABLE I. Annealing conditions used in our experiments.

Sample	Steel standard	Thickness (μm)	Anneal time (h)	Anneal condition
A	AISI 316	25.0		as received
B	AISI 316	12.5		as received
C	AISI 316	25.0	22	800 $^\circ\text{C}$ in air
D	AISI 316	12.5	22	800 $^\circ\text{C}$ in air
E	AISI 304	25.0	1	1050 $^\circ\text{C}$ in N_2

to a spherical dome with 38° field of view. After pressure was released, because of the elastic relaxation of the substrate, the height of the spherical dome was reduced to ~ 0.30 cm ($h/R=0.10$), corresponding to a 23° field of view. The 25- μm -thick foil was deformed less [Fig. 2(b), Sample A]. At 345 kPa, the center of 25- μm -thick foil was raised by ~ 0.40 cm ($h/R=0.13$), corresponding to a spherical dome with 30° field of view. After pressure was released, the height of the spherical dome was reduced to ~ 0.20 cm ($h/R=0.07$), corresponding to a 15° field of view. In these two cases, the field of view was reduced almost 50% after the elastic relaxation of the steel foils, which was not desirable because our goal was to permanently deform the substrate foil into a set spherical shape.

To reduce such elastic relaxation, it is essential to use substrates with lower yield strength. This was achieved by annealing the steel foils before deformation to create larger polycrystalline grains. Table I shows the annealing conditions used in our experiments (Sample E, AISI 304 stainless steel, was annealed by the supplier). Figure 2(a) demonstrates the effect of annealing on the measured stress–strain curves. Note for annealing at 800 $^\circ\text{C}$ or higher, the yield strength is reduced from ~ 0.8 GPa to ~ 0.2 GPa. Thus, annealed foils can be deformed with little elastic relaxation after pressure release [Fig. 2(b)]. For example, Sample E (annealed at 1050 $^\circ\text{C}$ in N_2 for 1 h) at 345 kPa, the center of the annealed foil was raised by ~ 0.93 cm ($h/R=0.31$), corresponding to a spherical dome with 69° field of view. After pressure was released, the height of the spherical dome was reduced to ~ 0.85 cm ($h/R=0.28$), corresponding to a 63° field of view. The height of the dome was only reduced by 8% due to the relaxation, which was a great improvement compared to the as-received foils [Fig. 2(b)]. Figure 3 shows the shape of the steel spherical dome (Sample E) after pressure was released, which closely matches that of an ideal spherical dome with 63° field of view.

B. Polyimide substrates

From the previous discussion, we demonstrated that it was easier to permanently deform substrates with lower yield strength. Plastic substrates in general have even lower yield strength compared to stainless-steel substrates. The height (measured from the center of the deformed foil) of 50- μm -thick KaptonTM Tab-E polyimide substrates (diameter = 6 cm) as a function of applied pressure is shown for both at room temperature [Fig. 4(a)] and at 150 $^\circ\text{C}$ [Fig. 4(b)] deformation. At room temperature, at 345 kPa, the center of the annealed foil was raised by ~ 1.05 cm ($h/R=0.35$). Af-

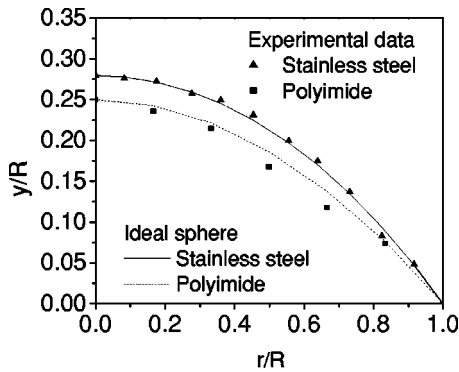


FIG. 3. Shape of a deformed 25- μm -thick stainless-steel sheet and a deformed 50- μm -thick polyimide substrate as a function of radius, with the height and radius normalized by the radius of the deformed region R (as defined in Fig. 1). Both stainless-steel and polyimide substrates were deformed at room temperature. The solid line (dotted line) represents an ideal spherical shape cap with the same height at the center of the stainless-steel (polyimide) cap in the experiments.

ter pressure was released, the height of the spherical dome was reduced to ~ 0.75 cm ($h/R=0.25$). Compared to the annealed 25- μm -thick stainless-steel foils [Sample E in Fig. 2(b)], the polyimide sample at room temperature was deformed more at 345 kPa ($h/R=0.35$ compared to h/R

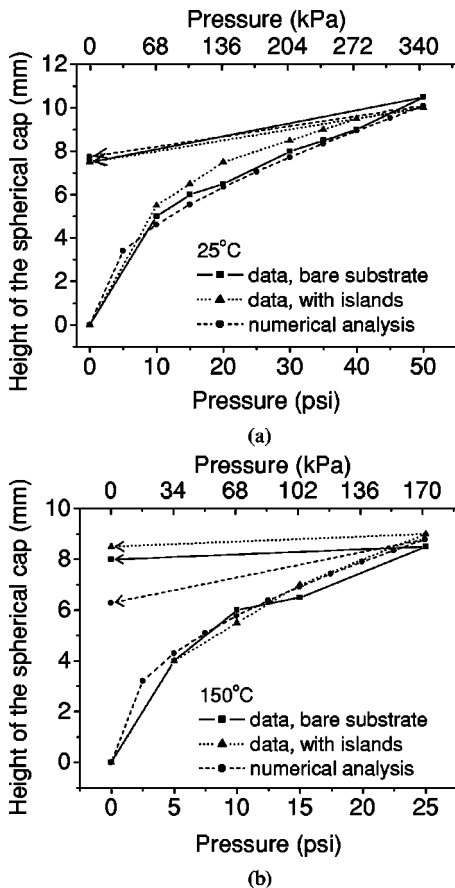


FIG. 4. Height of deformed polyimide substrates as a function of applied pressure at (a) room temperature and (b) 150 $^{\circ}\text{C}$. Height vs pressure predicted by numerical modeling is also presented. Also shown is height vs pressure for substrates with 20–100 μm islands (0.4- μm -thick silicon nitride followed by 0.1- μm -thick amorphous silicon) covering $\sim 25\%$ of surface area. The islands have little effect on the deformation profile.

TABLE II. Material parameters used in the numerical analysis.

	E (GPa)	σ_Y (GPa)	C (GPa)	n	Poisson ratio (ν)
Steel (AISI 304)	200	0.085	0.4	0.2	0.3
Polyimide room temperature	5	0.040	0.7	0.6	0.3
Polyimide 150 $^{\circ}\text{C}$	3	0.024	0.5	0.7	0.3

$=0.31$). However, the polyimide substrates have a larger relative change in h/R compared to the steel foil [Sample E in Fig. 2(b)] after the pressure release [final $h/R=0.25$ compared to $h/R=0.28$] because Young’s modulus of the polyimide substrate is 40 times smaller than that of the steel foil (Table II).

Heating up the polyimide substrate during deformation can further reduce its yield strength. For the sample deformed at 150 $^{\circ}\text{C}$, at 172 kPa (25 psi), the center of the annealed foil was raised by ~ 0.85 cm ($h/R=0.28$), corresponding to a spherical dome with 63 $^{\circ}$ field of view [the sample at room temperature had to be deformed at ~ 241 kPa (35 psi) to reach $h/R=0.28$]. After the pressure was released, the height of the spherical dome was reduced to ~ 0.80 cm ($h/R=0.27$), corresponding to a 60 $^{\circ}$ field of view [Fig. 4(b)]. Figure 3 shows the shape of the polyimide sample deformed at room temperature after pressure released, which closely matches that of an ideal spherical dome with 56 $^{\circ}$ field of view.

C. Strain distribution in the substrates

In contrast to previous works on clamped circular membrane deflections,^{7,8} the substrate was deformed plastically. The assumptions made in previous cases (the deflection was assumed to be small) were not valid,⁹ and the stress–strain equations for our substrates were not linear. Therefore, we used numerical modeling to examine the strain profile after deformation. We modeled the substrates used in the previous discussion as elastic–plastic materials with stress (σ)–strain (ϵ) relation as (Fig. 5)

$$\sigma = \begin{cases} E\epsilon, & \text{elastic, when } 0 < |\epsilon| < \sigma_Y/E \\ C\epsilon^n, & \text{plastic, when } \sigma_Y/E \leq |\epsilon| \end{cases} \quad (3)$$

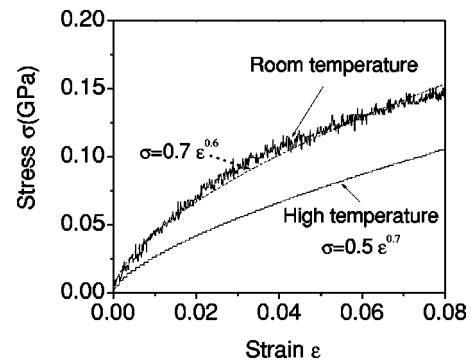


FIG. 5. Measured stress–strain curve for polyimide substrate at room temperature, and the predicted high-temperature stress–strain curve.

where n is the hardening index, C is a materials constant (derived from the curve fitting of the measured stress–strain relation), and E is Young’s modulus.¹⁰ σ_Y is the yield strength of the substrate, and is defined by the intersection of the elastic portion and the plastic portion of Eq. (3). We directly measured the stress–strain curves of Kapton™ E polyimide at room temperature (Fig. 5). For the mechanical properties of polyimide at 150 °C, we scaled the room-temperature properties according to the temperature dependence of the stress–strain relationship of a similar polyimide film (Kapton™ HN) available in the literature.¹¹ Table II summarizes the materials constants used in the numerical analysis.

We used a commercially available finite element analysis program, ABAQUS,¹² to calculate height versus pressure for a circular substrate clamped (6 cm in diameter) at its edge. The deformation was modeled as a perfect spherical cap in the cylindrical coordinates. Figures 4(a) and 4(b) show a comparison between the experimental data and the numerical modeling of height versus pressure for both room temperature and 150 °C. The results from a numerical analysis closely match the experimental data. This agreement gives us confidence that modeling the polyimide substrates as elastic–plastic materials [Eq. (3)], and the estimated 150 °C stress–strain curve are good assumptions.

The strain in the spherical dome is biaxial. At the top of the spherical dome, the value of the circumferential strain is equal to that of the radial strain because the stretching is uniform in all directions at the apex. Furthermore, the circumferential strain is fixed at zero at the edge of the spherical dome, due to the clamping condition at the boundary. Figure 6 shows the numerical modeling of the strain distribution in the substrate deformed into a 66° field of view ($h/R=0.29$). The deformation was modeled as a perfect spherical cap. The radial strain [Fig. 6(a)] for the stainless-steel foil is 7.5% at the top and gradually decreases to 2.3% at the clamped edge, with an average of 5.6%. For the polyimide substrate deformed at room temperature, the radial strain is 5.9% at the top and slowly decreases to 5.6% at the clamped edge, with an average of 5.7%. The radial strain is quite uniform across the spherical dome for the polyimide substrate. Note for $h/R=0.29$, simple geometric considerations [Eq. (2)] predicted an average radial strain of 5.6%.

III. SPHERICAL CAP DEFORMATION OF THIN-FOIL SUBSTRATES

A. Island concept

While polyimide and steel substrates can easily be plastically deformed with 6% strain, inorganic materials for semiconductor device structures such as silicon, silicon dioxide, and silicon nitride, can only be elastically deformed to a much lower value of strain before brittle fracture. To demonstrate this, 0.5- μm -thick silicon dioxide was deposited on a flat steel foil by spin casting a precursor and curing, and 0.4- μm -thick silicon nitride followed by 0.1- μm -thick amorphous silicon by plasma enhanced chemical vapor deposition at 150 °C on polyimide (the first layers for amorphous silicon transistor processing) were deposited onto flat polyimide

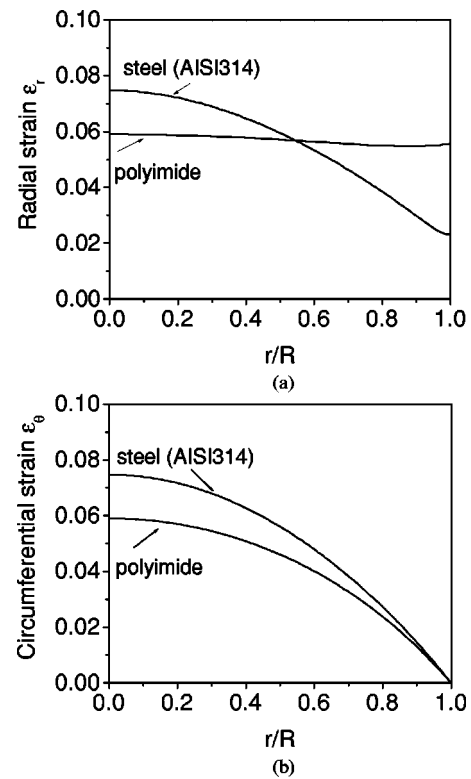


FIG. 6. (a) Radial strain and (b) circumferential strain distribution of the substrates (25- μm -thick stainless-steel and 50- μm -thick polyimide foil) deformed into a 66° field of view ($h/R=0.29$).

substrates. When the structures were then deformed into a 66° field-of-view spherical dome (with ~6% average radial strain), both the silicon dioxide on stainless steel and the silicon/silicon nitride on the polyimide substrate crack.⁶ This confirms that these hard materials cannot be expanded elastically or plastically to ~5% strain without failure.

We then patterned the stiff device materials into islands onto the compliant polyimide substrates with the hope that the large average strain in the substrate would not be transferred to the islands. The qualitative concept is that the soft substrate can flow beneath the island during the deformation so that the island itself might not be excessively strained (Fig. 7). This method was first applied to islands consisting of 0.5- μm -thick silicon dioxide on 25- μm -thick steel foil substrates. Only 5- μm -silicon dioxide islands remained intact after room-temperature deformation to a 66° field-of-view spherical dome. Because 5- μm -device islands are too small for amorphous silicon thin-film-transistor (TFT) fabri-

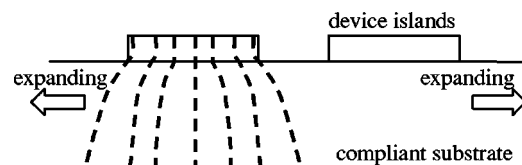


FIG. 7. Schematic diagram showing stiff islands on compliant substrates during deformation. Deformation takes place mostly in the interisland region to limit the strain in the substrates. The dotted lines represent deformation of originally straight vertical lines in the substrate.

cation in our lab, we turned to fabricating device islands on polyimide substrates.

B. Planar device islands on polyimide substrates

From the previous discussion, we know that by patterning uniform semiconductor layers into isolated islands, small islands can be fracture free after spherical deformation of the substrate. The blanket film of 0.1- μm -thick amorphous silicon and 0.4- μm -thick silicon nitride on a 50- μm -thick polyimide substrate was patterned before deformation into arrays of 20- to 120- μm -square islands, with the surface coverage varying from 4% to 44%. With this method, near the top of the spherical caps, intact square islands with a 20 μm edge, were routinely achieved after the substrate was deformed into a spherical dome with 66° field of view under pressure (56° field of view after pressure is released, corresponding to a height of ~ 0.75 cm). All larger islands cracked. In further experiments, TFTs were fabricated in these planar islands.¹³ We observed that the fracture of the TFTs typically took place first in the gate contact pad area, which was the thinnest region of the device (about ~ 0.5 μm thick).

Figure 4 compares the height versus pressure of the polyimide substrates with and without the islands, with an average surface coverage of 25%. Within experimental errors, the islands have no effect on deformation profiles and the resulting average strain in the substrate.

The device island has to be large enough for a transistor and three contact pads (source, drain, and gate) for characterization. We sought 40 μm islands for device fabrication. However, even at low island surface area coverage, it was not possible to realize 40 μm islands at room temperature without cracks [Fig. 8(b)]. We used two approaches to increase the island size. The first approach was to heat the substrate during deformation, and the second was to etch deep into the polyimide substrate to create a mesa island structure (see Sec. III C).

By heating the substrate to 150 °C to further soften the substrate during the deformation process, the maximum island size without cracks for deformation to a 66° field of view (before the pressure release) was increased to 100 μm . Figure 8(b) shows the yield (fraction of square amorphous silicon/silicon nitride islands on polyimide with no cracks) of the islands without cracks versus island size near the top of the cap where the strain is the highest. In experiments, varying the spacing between the islands to change the island density has little effect on the yield of crack-free islands for room-temperature deformation. For 150 °C, it has little effect when the island density is larger than 10%. It is due to the fact that once the substrate begins to plastically deform, further strain requires very little additional stress. Consequently, the shear load that pulls the island is only weakly dependent on the area of the interisland region, and the island density is not a substantial factor in the fracture mechanism.

C. Mesa device islands on polyimide substrates

Though most 50- μm -planar islands (with a few 100 μm ones) deformed at 150 °C were intact after deformation, because of the instability of amorphous silicon, it was not de-

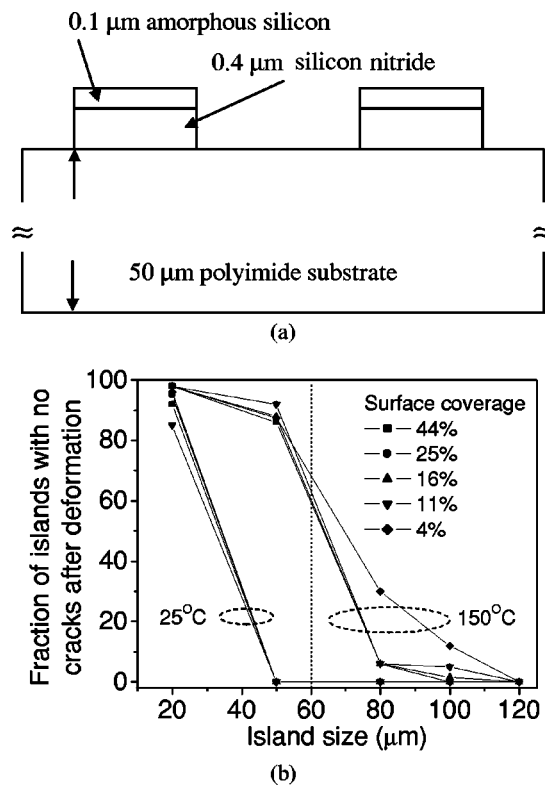


FIG. 8. (a) Cross section of planar island structure. (b) Fraction of square amorphous silicon/silicon nitride islands on polyimide with no cracks as a function of the island length, for different surface area coverage. Substrate is deformed to 66° field of view at room temperature or 150 °C. The data were taken near the center of the cap.

sirable to deform the final device structure at high temperature. To achieve the maximum island size without fracture after deformation at room temperature, we developed an alternative structure, in which we not only pattern the semiconductor material into individual islands but also etch deep (~ 10 μm) into the substrate to create the device on a polyimide mesa structure [Fig. 9(a)]. The sidewalls of these compliant polyimide mesas could withstand the large shear stress from the substrate expansion. These mesa pillars protected device islands from the substrate so that the strain in the device islands was greatly reduced. While only 20- μm -planar islands were intact after the substrate was deformed to a 66° field-of-view spherical dome at room temperature, $\sim 50\%$ of the 80- μm -mesa islands (25% surface area coverage) deformed at room temperature were intact after deformation [Fig. 9(b)]. Mesa islands deformed at room temperature also have a higher yield compared to the planar islands deformed at 150 °C. Only $\sim 5\%$ of the 80- μm -planar islands (with surface area coverage of 25%), deformed at 150 °C, were intact after deformation.

IV. STRAIN DISTRIBUTIONS IN ISLAND STRUCTURES

A. Modeling of strain distribution in the islands

In this section, we use numerical modeling to calculate the strain distribution in the islands. This is desired to understand the performance of the TFTs after deformation in those islands.¹³ Four important approximations are made in per-

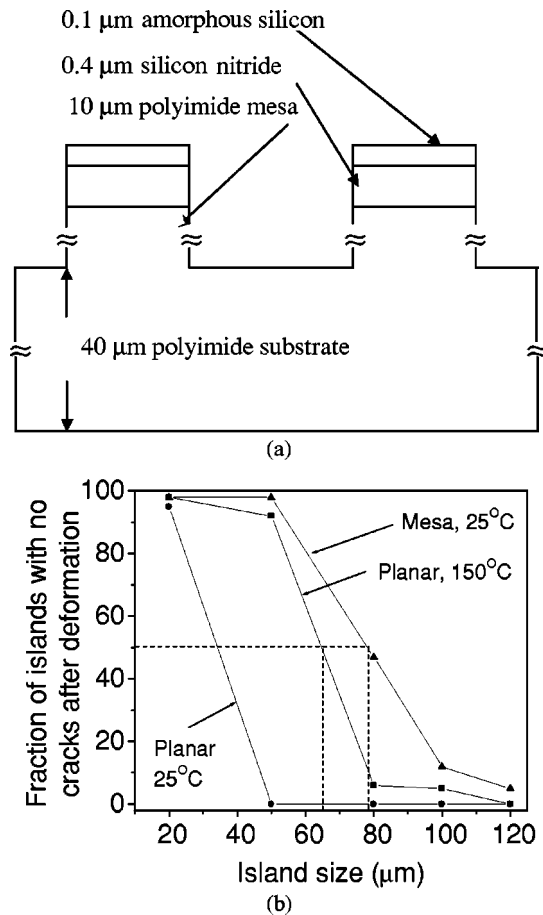


FIG. 9. (a) Cross section of mesa island structure. (b) Fraction of square amorphous silicon/silicon nitride islands on polyimide with no cracks as a function of the island length, for 25% surface area coverage. Substrate is deformed to 66° field of view at room temperature. The data were taken near the center of the cap.

forming this calculation. First, we seek in detail the strain distribution of one island at the top of the spherical cap, where the strain is the greatest. The effect of the local bending curvature due to the spherical deformation on the strain is negligible at the apex of the dome, because the islands are very small compared to the entire substrate. (These islands are of magnitude of 100 μm wide, and the radius of curvature of the substrate is ~5 cm). Consequently, nearly all of the strain will come from the biaxial stretching of the substrate caused by expansion in both radial and circumferential directions. The dimension of the numerical modeling is thus reduced to a two-dimensional problem. Second, from experimental data, we learned that the island surface area coverage had little effect on the yield of the intact islands. This suggests that the stress on the island is only weakly dependent on the island spacing. Therefore, for most of the numerical modeling, we only consider one single island and its immediate surrounding substrate. Third, from Sec. II C, we concluded that the radial strain in the plastic substrate is quite uniform [Fig. 6(a)], and the peak strain is close to the average radial strain predicted by Eq. (2). Hence, we model this single island on the top of the dome as an island stretched with an average radial strain of the value equal to the average radial strain across the spherical cap calculated from the

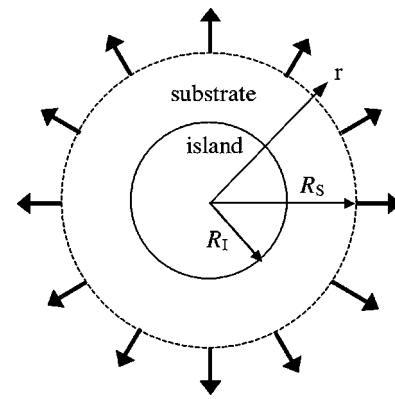


FIG. 10. Schematic diagram (top view) of the modeled round island (radius R_I) and substrate (radius R_S) in the numerical modeling. Biaxial strain is applied radially outward from the edge of the substrate.

height of deformation [Eq. (2)]. Finally, for simplicity, we model device islands as a single round (not square as in experiments) island with radius R_I . The island is surrounded by a circle of bare substrate (radius R_S), the edges of which are expanded radially by a fixed amount as a boundary condition of the simulation. The surface area coverage (island density) is thus $(R_I/R_S)^2$ (Fig. 10).

To implement the modeling, we used ABAQUS¹² to examine the strain distribution in the thin-film island/substrate structure. Planar islands are 0.5 μm thick and mesa islands are 1 μm thick, unless otherwise noted. The polyimide substrate is 50 μm thick with the stress-strain relation described in Eq. (3) and the material parameters in Table II. We assume Young's modulus for all device layers to be 200 GPa.¹⁴ We also assume that the substrate (radius R_S) is stretched with 6% strain (corresponding to $h/R=0.30$) in the radial direction when the pressure is on. In our experiments, the height of the spherical dome deformed at room temperature was reduced to $\sim h/R=0.25$ {corresponding average radial strain [$\epsilon_{r,avg}$ of 4.0%, Eq. (2)]} after the pressure release. At 150°C, these figures were $h/R=0.27$ and $\epsilon_{r,avg}=4.7\%$, respectively.

Therefore, after stretching the substrate by 6%, in our modeling, we reduced substrate stretching to 4% in the radial direction for room-temperature deformation to find the final strain distribution in the islands after pressure release. For 150°C deformation, we relaxed the substrate stretching to 5% to study the final strain distribution in the islands after pressure release.

B. Strain distribution in planar islands

Figure 11 shows a contour plot of the radial strain distribution in a structure with 100-μm-diameter planar island after stretching to 6% at the substrate boundary at room temperature (before being allowed to relax back to 4% stretching). The results show that the strains are pinned to low values in the island and the nearby substrate by the high Young's modulus of the island, but increase farther from the island and deep underneath it. This confirms the qualitative concept of the islands described in Fig. 7. Indeed, for the rigid islands to be intact, the plastic deformation must occur

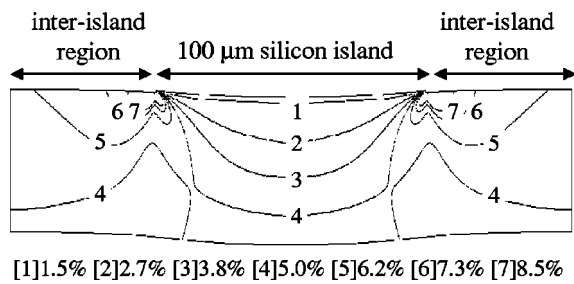


FIG. 11. Contour plot of the radial strain distribution in a 50- μm -thick polyimide substrate with a round silicon island (100 μm in diameter) of 0.5 μm thick after stretching to average biaxial tension of 6% at room temperature. The modeled substrate size was a circle of 200 μm in diameter.

in the substrate region farther away from the islands. Figure 12 shows the radial strain in a round 1- μm -thick 50- μm -diameter amorphous silicon island as a function of position after deformation at 150 $^{\circ}\text{C}$ to 6% average strain and then relaxation back to 5% average strain in the substrate. Note that the radial strain is largest (0.33% when pressure is on, 0.29% when pressure is off) at the island center and gradually decreases to near zero toward the island edge. Figure 13 shows the calculated radial strain at the center of the island as a function of the island diameter for 0.5- μm -thick silicon planar (island density ranging from 6.2% to 60%) and mesa islands (before relaxation) on a 50- μm -thick polyimide substrate stretched with 6% strain for room-temperature deformation. The strain in the islands increases as a function of the island diameter, explaining why larger islands crack. The strain in the island is a weak function of the island density, consistent with the experimental observation that the surface area coverage does not affect the yield of islands without cracks.

C. Strain distribution in mesa islands

Figure 13 suggests that mesa islands indeed have a much lower strain than planar islands of similar geometry, which explains the experimental realization of larger intact islands with this approach. In the experiment, $\sim 50\%$ of 80- μm -mesa islands do not fracture after the substrate deformed to a spherical dome with a 66° field of view ($h/R=0.29$), when

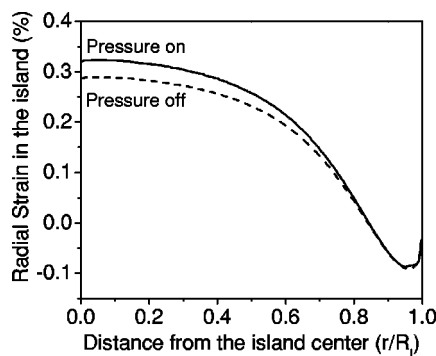


FIG. 12. Predicted radial strain in a round amorphous silicon island (thickness=1 μm , diameter=50 μm) after the polyimide substrate (50 μm thick) is deformed with 6% strain and relaxed to 5% strain in the substrate as a function of position, using the estimated 150 $^{\circ}\text{C}$ mechanical properties of polyimide of Table II.

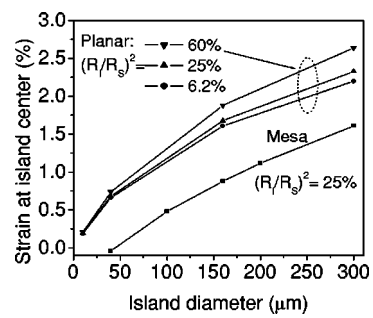


FIG. 13. The maximum strain in the islands as a function of the island diameter for 0.5- μm -thick circular silicon islands (both planar and mesa islands) on a 50- μm -thick polyimide substrate stretched with 6% strain at room temperature.

the pressure was on [Fig. 9(b)]. Modeling shows for mesa islands of 80 μm , the strain at the center of the island is larger than 0.3% [Fig. 13]. We conclude that the critical strain at which the islands break is approximately 0.3%. This is consistent with previous results in which amorphous silicon TFTs were subject to uniaxial tension by cylindrical deformation.^{4,5} Figure 13 also implies that for mesa islands smaller than 40 μm , the strain at the island center is smaller than zero when the pressure was on, implying that the island centers were in compression. That the island could be in compression after stretching the substrate is surprising, however, the phenomenon was also observed when measuring the TFT device characteristics of TFT on mesa structure.¹⁵ To understand this, Fig. 14 shows the modeled radial strain as a function of radius in a round amorphous silicon island (thickness=1 μm , diameter=50 μm) on 10- μm -polyimide mesa after the polyimide substrate (50 μm thick) is deformed with 6% strain and relaxed to 4% average strain. It shows that the island center is under compression with compressive strain of $\sim -0.09\%$ when pressure is applied. After the pressure is released, the strain is decreased algebraically to $\sim -0.11\%$. The compression can be explained by the cross sections of the structure at different stages of the finite element analysis (Fig. 15). During deformation, the strain at the side of the polyimide pillars was so large that the lower mesa edge was permanently deformed. After the releasing the pressure, the mesa edge was still bent. Consequently, the

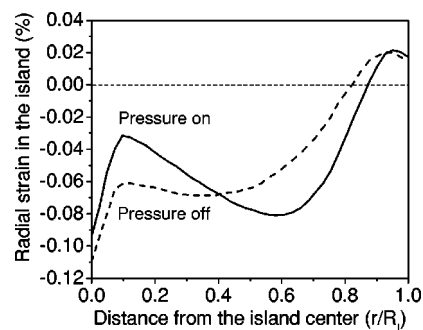


FIG. 14. Predicted radial strain in a round amorphous silicon island (thickness=1 μm , diameter=50 μm) on 10- μm -polyimide mesa after the polyimide substrate (50 μm thick) is deformed with 6% strain and relaxed to 4% strain in the substrate as a function of position, using the room-temperature mechanical properties of polyimide of Table II.

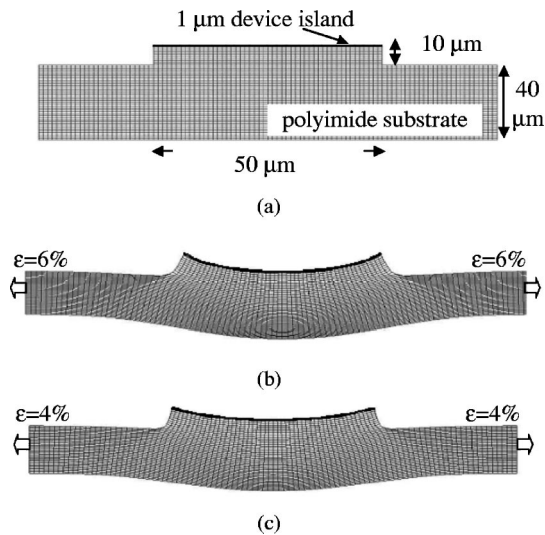


FIG. 15. Structure of a 50- μm -round amorphous silicon island (thickness = 1 μm) on 10- μm -polyimide mesa: (a) Before deformation and (b) during deformation (to 6% strain at the substrate boundary). The deformation at mesa edge is permanent, and (c) after pressure release (4% strain at the substrate boundary).

island center was forced into compression even though the substrate as a whole on average was in tension. Note that the performance of amorphous silicon TFTs on mesa structures after deformation is consistent with that films being in compression (a reduction in mobility). The relationship between device performance and the island structure is examined in detail in another publication.¹⁵

For applications, such as displays on objects with arbitrary shapes, the substrate can be repeatedly deformed with different strain levels. Thus, it is highly desirable to fabricate devices with structures less sensitive to the substrate deformation to assure consistent electronic characteristics. Figure 16 shows the calculated radial strain at the island center as a

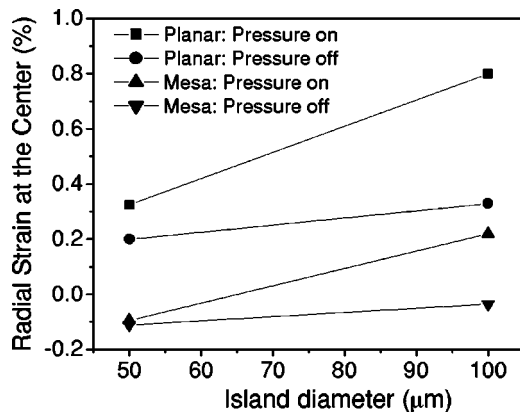


FIG. 16. Predicted strain at the island center as a function of the island diameter for 1- μm -thick circular silicon islands (both planar and mesa islands) on a 50- μm -thick polyimide substrate stretched with 6% strain at the substrate boundary when pressure is on and after pressure release (4% strain at the substrate boundary) at room temperature. The island density is 50%.

function of the island diameter for 1- μm -thick circular silicon islands (both planar and mesa islands) on a 50- μm -thick polyimide substrate stretched with 6% strain at the substrate boundary when pressure is on and after pressure release (4% strain at the substrate boundary) at room temperature. Note that by using a mesa design, it is feasible to design devices so that these devices endure little strain during the substrate deformation.

V. SUMMARY

In summary, we have investigated the material basis for developing spherically shaped electronics by deforming thin foil substrates with prefabricated device structures. Unlike previous work in cylindrical deformation, ultrathin substrates cannot reduce the large average strain in the substrate, which is caused by the spherical deformation. Spherical deformation requires use of device islands on compliant substrates to enable device regions to withstand strain without cracking during deformation. The strain in the island increases with the island size, but is only weakly dependent on island density when the substrate is soft. By etching into the substrate to create TFTs on a polyimide mesa device structure, the strain in the device layers was greatly reduced. Furthermore, the devices could be in compression even if the substrate was stretched due to the plastic deformation at the polyimide island edge.

ACKNOWLEDGMENTS

The authors gratefully acknowledge the support from DARPA/ONR (Grant No. N60001-98-1-8916), New Jersey Commission on Science and Technology, and Princeton Plasma Physics Laboratory.

- Y. Chen, J. Au, P. Kazlas, A. Ritenour, H. Gates, and J. Goodman, *Tech. Dig. - Int. Electron Devices Meet.* **2002**, 389 (2002).
- M. G. Kane, J. Campi, M. S. Hammond, F. P. Cuomo, B. Greening, C. D. Sheraw, J. A. Nichols, D. J. Gundlach, J. R. Huang, C. C. Kuo, L. Jia, H. Klauk, and T. N. Jackson, *IEEE Electron Device Lett.* **21**, 534 (2000).
- J. Engel, J. Chen, C. Liu, B. R. Flachsbar, J. C. Selby, and M. A. Shannon, *Mater. Res. Soc. Symp. Proc.* **736**, D.4.5.1 (2003).
- Z. Suo, E. Y. Ma, H. Gleskova, and S. Wagner, *Appl. Phys. Lett.* **74**, 1177 (1999).
- H. Gleskova, S. Wagner, W. Soboyejo, and Z. Suo, *J. Appl. Phys.* **92**, 6224 (2002).
- P. I. Hsu, M. Huang, S. Wagner, Z. Suo, and J. C. Sturm, *Mater. Res. Soc. Symp. Proc.* **621**, Q8.6.1 (2000).
- S. Timoshenko and S. Woinowsky-Krieger, *Theory of Plates and Shells*, 2nd ed. [McGraw-Hill, New York, 1987].
- A. Hermida, *NASA Tech Briefs* **22**, 78 (1998).
- L. Howell, *Compliant Mechanisms* (Wiley, New York, 2001).
- A. Kreuz, S. N. Milligan, and R. F. Sutton, *DuPont Films Technical Paper No. 3/94*, Reorder No. H54504.
- DuPont Films Technical Paper 8/97, Reorder No. H-38492-2.
- ABAQUS, Version 5.8 (Hibbit, Karlsson, and Sorensen, Inc., Rhode Island, 1999).
- P. I. Hsu, R. Bhattacharya, H. Gleskova, M. Huang, Z. Xi, Z. Suo, S. Wagner, and J. C. Sturm, *Appl. Phys. Lett.* **81**, 1723 (2002).
- F. Jansen and M. A. Machonkin, *J. Vac. Sci. Technol. A* **6**, 1696 (1988).
- P. I. Hsu, M. Huang, H. Gleskova, Z. Xi, Z. Suo, S. Wagner, and J. C. Sturm (unpublished).